Scilight

New Energy Materials and Devices
https://www.sciltp.com/journals/nemd



Review

Check for updates

Phosphate Chemistry for Zinc Anode Protection in Aqueous Batteries

Xiaoyan Li, Zhongyuan Wang, Tianrui Guan, Yingjin Wei * and Yizhan Wang *

Key Laboratory of Physics and Technology for Advanced Batteries (Ministry of Education), State Key Laboratory of Superhard Materials, College of Physics, Jilin University, Changchun 130012, China
* Correspondence: yjwei@jlu.edu.cn (Y.W.); wangyizhan@jlu.edu.cn (Y.W.)

How To Cite: Li, X.; Wang, Z.; Guan, T.; et al. Phosphate Chemistry for Zinc Anode Protection in Aqueous Batteries. *New Energy Materials and Devices* **2027**. https://doi.org/10.53941/nemd.2027.100001

Received: 15 September 2026
Revised: 20 October 2026
Accepted: 6 November 2026
Published: 18 November 2026

Abstract: Aqueous zinc metal batteries are an appealing option for safe, low-cost energy storage, yet the poor reversibility of Zn metal remains a practical barrier. Near the anode, corrosion, hydrogen evolution, interfacial precipitation and nonuniform deposition are tightly intertwined through the local water environment and Zn^{2+} transport. Phosphate chemistry is well suited to regulating these processes, since phosphate can move from dissolved species in the electrolyte to protective phases on the Zn surface, and further into functional components of quasi-solid networks. This review follows that progression, treating phosphate-enabled Zn protection along a solution-to-interface continuum. We begin with how phosphate speciation and Zn^{2+} association shape the local electrolyte environment, then examine how these interactions give rise to phosphate-containing interphases, and finally consider their extension into quasi-solid ion-transport networks. In each regime, the same tension recurs: phosphate chemistry must suppress water-driven side reactions without impeding Zn^{2+} transfer. We argue that the design principle is not to maximize coordination or passivation, but to control the chemical state and spatial evolution of phosphate so that interfacial protection and Zn^{2+} transport remain balanced.

Keywords: aqueous zinc metal batteries; phosphate chemistry; solvation regulation; functional interphase; ion-conducting network

1. Introduction

Aqueous zinc metal batteries are promising for large-scale electrochemical energy storage: water-based electrolytes offer high ionic conductivity and low flammability, while Zn metal combines high capacity, natural abundance and low cost [1]. Metallic Zn has theoretical capacities of 820 mAh g^{-1} and 5855 mAh cm^{-3}, together with a redox potential of approximately −0.76 V versus the standard hydrogen electrode. These values make aqueous Zn systems attractive where safety, cost and resource availability are the main concerns. Their practical viability, however, depends on whether Zn can undergo highly reversible plating and stripping under finite Zn inventory, limited electrolyte and practically relevant areal capacities.

The central difficulty is the direct contact between highly reducing Zn metal and water. During Zn deposition, solvated Zn^{2+} must approach and discharge at a surface where water reduction and chemical corrosion can occur simultaneously [2,3]. These reactions consume active Zn and electrolyte, generate hydrogen and shift the local acid-base balance. The resulting precipitates and surface heterogeneity redistribute ion flux and current density, favoring uneven deposition and porous Zn growth [4]. During subsequent stripping, electrically isolated Zn and freshly exposed reactive sites can be left behind, further accelerating interfacial degradation. These failure pathways reinforce one another rather than acting independently. Recent work on aqueous Zn batteries has emphasized the need for Zn protection against corrosion, hydrogen evolution and nonuniform deposition [5−14].

Copyright: © 2026 by the authors. This is an open access article under the terms and conditions of the Creative Commons Attribution (CC BY) license (https://creativecommons.org/licenses/by/4.0/).
Publisher's Note: Scilight stays neutral with regard to jurisdictional claims in published maps and institutional affiliations.

Effective protection must suppress water-driven reactions while preserving fast, spatially uniform Zn^{2+} transfer. The trade-off is intrinsic: stronger isolation from water improves chemical stability, but excessive passivation impedes ion transport and increases interfacial polarization.

Phosphate chemistry is well suited to managing this trade-off because its role changes with the local chemical environment. In solution, phosphate-containing species interact with Zn^{2+} and alter the organization of water in the Zn^{2+} coordination shell. Their protonation state also responds to local pH, which is continuously perturbed during Zn plating and stripping. As phosphate accumulates near the electrode, changes in Zn^{2+} activity and proton concentration can strengthen ion association and eventually promote interfacial precipitation or conversion into Zn-phosphate-containing phases. Phosphate can therefore link solution regulation to interphase formation rather than acting only as an electrolyte additive or a passive coating. The same interaction that improves interfacial stability can become detrimental when too strong: excessive Zn^{2+} coordination slows ligand exchange, and uncontrolled precipitation produces a resistive layer. The useful window lies between too little interaction and over-immobilization, where water-driven reactions are suppressed without sacrificing Zn^{2+} transfer. Previous reviews have mainly addressed Zn-anode stabilization through electrolyte engineering, electrode modification and separator design [4], zinc salt chemistry [15], aqueous solvation regulation [16], electrolyte additives [17,18] and protective interphases [19,20]. This review instead develops a chemical-state-dependent mechanistic framework that links phosphate speciation, Zn^{2+} coordination and local pH to interphase formation or reconstruction and to ion transport in quasi-solid environments. The aim is to show how the chemical state and spatial distribution of phosphate influence the balance between interfacial protection and Zn^{2+} transport.

Phosphate-based electrolyte regulation [21] and preconstructed phosphate-containing interphases [22,23] have been demonstrated, and related quasi-solid interphase and polymer electrolyte strategies [24,25] underline the need for efficient ion-transport pathways. Broader advances in aqueous energy-storage cathodes [26,27], Zn battery materials and device design [28], electrolyte regulation [29] and interfacial engineering [30] provide additional context. What is still lacking, however, is a phosphate-centered account that connects solution chemistry, interphase formation and quasi-solid environments. This review therefore organizes phosphate-enabled Zn protection along a solution-to-interface continuum. We examine phosphate speciation, Zn^{2+} association and water regulation in the electrolyte; then discuss the formation and evolution of phosphate-containing interphases; and finally consider their extension into quasi-solid and networked electrolytes. These regimes are not a universal sequence of chemical transformations. They are connected by interactions among phosphate species, Zn^{2+} and water. This framework provides a mechanistic basis for distinguishing effective phosphate protection from excessive coordination or passivation, and for guiding the design of reversible aqueous Zn metal anodes.

2. Solution-State Phosphate Chemistry for Zn Anode Regulation

Phosphate regulation starts in the electrolyte, before any solid interphase forms. During Zn plating, Zn^{2+} consumption and local OH^- generation make the reaction environment near the electrode quite different from the bulk solution. Phosphate species respond through protonation, association with Zn^{2+}, and redistribution near the electrode [31–35]. As the local environment changes, soluble phosphate can shift from a weak solution regulator to a precursor for interfacial phosphate formation [36–43]. This solution-to-interface evolution is the chemical basis for understanding how phosphate affects both Zn^{2+} transfer and subsequent surface protection.

2.1. Phosphate Speciation and Zn^{2+} Association

Phosphates and related phosphorus-containing compounds can be classified according to their molecular structures and coordination characteristics. Inorganic phosphates exhibit pH-dependent protonation equilibria, with increasingly deprotonated species showing stronger Zn^{2+} association and a greater tendency toward zinc phosphate precipitation. In contrast, neutral phosphate esters, such as trimethyl phosphate and triethyl phosphate, mainly regulate Zn^{2+} solvation and the local water environment through their phosphoryl groups. Phosphonates contain direct P–C bonds and may provide strong metal coordination or surface anchoring when ionizable phosphonic acid groups are present, whereas fully esterified phosphonates can behave differently. Phytate derivatives, which contain multiple phosphate ester groups, offer multidentate coordination sites that facilitate interfacial adsorption and the formation of Zn-containing networks. The solubility, coordination strength, and interfacial behavior depend on their ionization states, concentrations, and electrolyte environments.

Among these classes, inorganic phosphate species undergo protonation equilibria that are strongly influenced by the local acid–base environment, giving rise to H_3PO_4, $H_2PO_4^-$, HPO_4^{2-}, and PO_4^{3-} with different charge densities and Zn^{2+} affinities [44–49]. In the mildly acidic electrolytes commonly used for aqueous Zn metal batteries, protonated phosphate species can dominate in the bulk. During cathodic polarization, however, proton

consumption and water reduction increase the local pH, shifting the equilibrium toward more deprotonated forms. This shift directly changes the behavior of phosphate near Zn. Greater deprotonation generally strengthens electrostatic interactions with Zn^{2+} and can alter its local coordination environment. At the same time, protonation–deprotonation reactions moderate the pH excursion generated during plating [50–55]. The speciation and interfacial behavior of inorganic phosphates are therefore dynamically coupled to the electrode reaction rather than fixed by the initial bulk composition.

For inorganic phosphate species, stronger local association with Zn^{2+} can promote a transition from soluble complexes toward clustering and, under supersaturated conditions, solid formation. This transition is controlled by local ion activities rather than bulk concentration alone [56−61]. A moderate level of association can modify the environment surrounding Zn^{2+} without removing it from the mobile electrolyte. Once local supersaturation is reached, however, Zn-phosphate-containing phases may nucleate near the electrode. Such interfacial formation can be protective when spatially confined, but excessive precipitation can instead produce a resistive layer or even bulk turbidity. Before precipitation, Zn^{2+} and phosphate can associate through solvent-separated, solvent-shared, or direct-contact configurations. These configurations differ in how much water remains between Zn^{2+} and the phosphate oxygen atoms and therefore in the extent to which the Zn^{2+} solvation environment is perturbed [42,43]. Such interactions can modify the hydration environment and ligand exchange involved in interfacial Zn^{2+} transfer, although stronger coordination does not necessarily lead to faster transport. The useful regime is therefore not the strongest possible Zn^{2+}-phosphate interaction, but a sufficiently labile association that modifies the local solvation environment while preserving rapid Zn^{2+} exchange [62–65]. This balance is strongly dependent on phosphate concentration, protonation state, competing anions, and the evolving interfacial environment. It also determines whether phosphate remains a solution regulator or begins to form a protective solid at the Zn surface.

2.2. Solvation and Interfacial Water Regulation

Phosphate-containing molecules can regulate Zn deposition before a solid interphase is formed by changing the local environment of Zn^{2+} and water. Their effect depends on how strongly they enter the Zn^{2+} coordination environment and how readily they exchange with water. Moderate interaction can reduce direct exposure of Zn to reactive water while preserving the ligand exchange required for Zn^{2+} transfer. This balance is illustrated by phosphate esters such as trimethyl phosphate (TMP). Tu et al. demonstrated that TMP can regulate the Zn^{2+} coordination environment and water hydrogen-bonding network in $ZnSO_4$ electrolytes [21]. These changes were accompanied by suppressed Zn corrosion, more uniform deposition, and improved cycling stability in both Zn||Zn symmetric and Zn||V_2O_5 full cells. This study illustrates how molecular phosphate regulators can improve Zn reversibility by modifying the local solution environment and mitigating interfacial side reactions.

This behavior is not unique to TMP. Other phosphate-containing molecules can also influence Zn^{2+} coordination and the local water environment through their P–O groups, although the dominant effect varies with molecular structure [62–64]. Phosphate esters, phosphonates, and phytate derivatives differ in charge, steric environment, and affinity for both Zn^{2+} and the electrode surface. As a result, similar improvements in cycling stability do not necessarily arise from the same molecular mechanism. Concentration is particularly important in determining where phosphate regulation occurs. At low concentrations, phosphate-containing molecules are more likely to act through preferential adsorption or interfacial enrichment. At higher concentrations, they can more strongly perturb the bulk coordination environment and water structure, but may also increase viscosity or slow ligand exchange [66–75]. The optimum composition therefore reflects a balance between sufficient regulation and preservation of Zn^{2+} mobility. Spectroscopic changes associated with water should also be interpreted carefully. A shift in the O–H stretching band demonstrates a change in hydrogen-bonding environment, but does not directly quantify water activity or electrochemical reactivity. Likewise, NMR, thermal analysis, and thermodynamic activity measurements describe different aspects of water behavior [76–82]. For Zn protection, the most relevant effect is the reduction of reactive water near the metal without excessively restricting Zn^{2+} transport. Molecular phosphate regulators therefore mainly act by reshaping the local solution environment before Zn reaches the electrode. As phosphate becomes more ionic and more strongly coupled to acid–base equilibria, however, another level of regulation emerges.

Inorganic phosphates provide a complementary route to Zn-anode regulation by responding directly to the local acid–base environment. During Zn plating, proton consumption and water reduction can increase the interfacial pH, promoting the formation of poorly soluble by-products. Liu et al. introduced diammonium hydrogen phosphate (DAP) to moderate this local change [50]. The DAP-containing electrolyte exhibited reduced pH fluctuations, more uniform Zn deposition, and enhanced preferential Zn(002) orientation. These results suggest that phosphate regulation modifies both the local interfacial environment and Zn crystallographic texture. Zhang

et al. further demonstrated the effectiveness of ammonium dihydrogen phosphate (NHP) in stabilizing the electrolyte pH during Zn plating and stripping [51]. As illustrated in Figure 1a,b, NHP was proposed to suppress interfacial side reactions through the combined effects of pH buffering and NH_4^+ adsorption. In the acid-adjusted control electrolyte (S-BE), pronounced pH fluctuations were observed during cycling (Figure 1c), accompanied by premature short-circuit failure after approximately 60 h (Figure 1d). In contrast, the NHP-containing electrolyte (DE) maintained a relatively stable pH (Figure 1e), enabling stable Zn||Zn cycling for approximately 315 h at 5 mA cm^{-2} and 5 mAh cm^{-2} (Figure 1f). These results highlight the importance of dynamic pH regulation, rather than simply adjusting the initial electrolyte pH, in suppressing interfacial degradation and improving Zn reversibility.

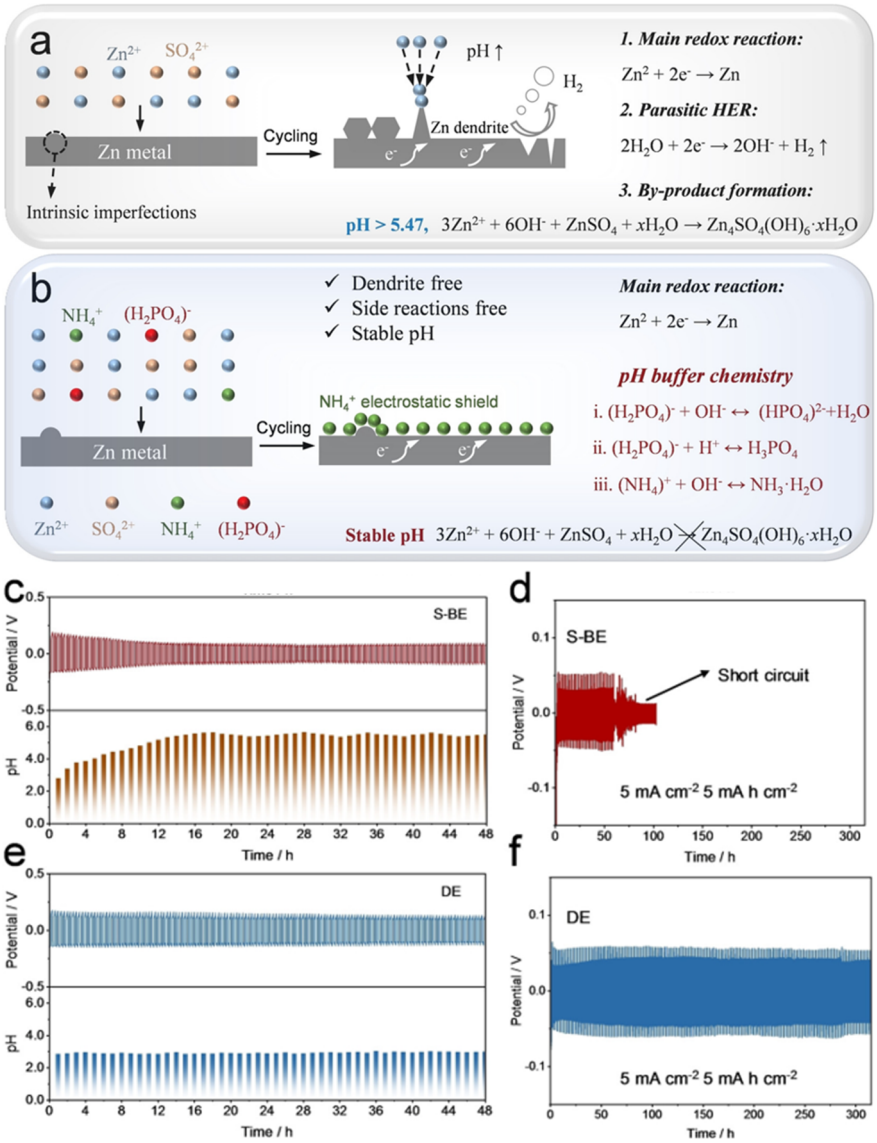

Figure 1. The schematic diagram of zinc plating processes in (**a**) 1 M $ZnSO_4$ (BE) and (**b**) 1 M $ZnSO_4$ + 25 mM NHP (DE). *In Situ* pH monitoring of (**c**) 1 M $ZnSO_4$ + xH_2SO_4 (S-BE), and (**e**) 1 M $ZnSO_4$ + 25 mM NHP (DE) within Zn//Zn symmetric cells upon cycling at 10 mA cm^{-2}. Cycling performances of Zn//Zn symmetric cells in, (**d**) 1 M $ZnSO_4$ + xH_2SO_4 (S-BE), and (**f**) 1 M $ZnSO_4$ + 25 mM NHP (DE) at 5 mA cm^{-2}/5 mAh cm^{-2}. Reproduced with permission from Ref. [51]. Copyright 2023 Wiley-VCH GmbH.

The beneficial effect of inorganic phosphate exists within a limited composition window. Insufficient phosphate provides little resistance to local pH changes, whereas excessive deprotonated phosphate can increase Zn^{2+} association and drive zinc-phosphate precipitation. Once precipitation becomes extensive, Zn^{2+} may be depleted from the mobile electrolyte and a resistive deposit can develop. Acid adjustment can maintain bulk electrolyte stability, but the interfacial speciation can still shift during polarization because the local environment differs from the bulk. Effective regulation therefore requires phosphate to remain sufficiently soluble in the electrolyte while retaining the ability to respond locally at the Zn surface. This balance is also reflected in other inorganic phosphate systems [83−86]. Solution-state phosphate regulation spans a gradual transition from soluble

interaction to interfacial solid formation. Effective protection requires Zn^{2+} to remain sufficiently mobile in the bulk while stronger phosphate interactions are confined to the electrode vicinity. Representative phosphate-containing electrolyte regulators and their reported electrochemical performance are summarized in Table 1.

Table 1. Quantitative comparison of representative phosphate-containing electrolyte regulators for aqueous Zn anodes.

Regulator	Reported Function	Zn Symmetric Test	Full-Cell/Practical Result	Ref.
Trimethyl phosphate	Solvation and H-bond perturbation	>3000 h @ 1 mA cm^{-2}/ 0.5 mAh cm^{-2}	V_2O_5: 66 mAh g^{-1} after 1000 cycles @ 1 A g^{-1}; cathode loading: 1–2 mg cm^{-2}	[21]
$(NH_4)_2HPO_4$	pH buffering + H-bond disruption + Zn(002)	>5300 h @ 5 mA cm^{-2}/ 0.5 mAh cm^{-2}; 500 h @ 30 mA cm^{-2}/ 10 mAh cm^{-2}	MnO_2: 99.9% retention after 200 cycles @ 1 A g^{-1}; cathode loading: 1–1.5 mg cm^{-2}; N/P ratio: 479–719; areal capacity: 0.16–0.24 mAh cm^{-2}	[50]
beta-Glycerophosphate Na	Solvation + adsorption + Na^+ shielding	>1900 h @ 0.5 mA cm^{-2}/ 0.25 mAh cm^{-2}; >1200 h @ 5 mA cm^{-2}/ 2 mAh cm^{-2}	NHVO full cell: 800 cycles; N/P rario: 9.5; areal capacity: 6.2 mAh cm^{-2}; electrolyte amount: 70 μL	[62]
Trimethyl phosphate	Solvation-shell reshaping; water-network regulation	>7000 h @ 1 mA cm^{-2}/ 0.5 mAh cm^{-2}	VO_2(B): 97.86% after 1200 cycles @ 1 A g^{-1}; cathode loading: 1.5 mg cm^{-2}; N/P ratio: 156; areal capacity: 0.375 mAh cm^{-2}; electrolyte amount: 120 μL	[63]
Phytate ammonium	Adsorption/NH_4^+ shielding	>2000 h @ 5 mA cm^{-2}/ 1 mAh cm^{-2}	V_2O_5: 115.2 mAh g^{-1} of 200 cycle@ 2 A g^{-1}; cathode loading:1 mg cm^{-2}; N/P ratio: 28.4	[67]
Triethyl phosphate	Compact interphase; EDL and Zn(002) regulation	>5000 h @ 1 mA cm^{-2}/ 1 mAh cm^{-2}	LFP: 116.0 mAh g^{-1} @ 1 C; cathode lading: 1 mg cm^{-2}; N/P ratio: 505; electrolyte amount: 147 μL cm^{-2}	[68]
Trimethyl phosphate	Solvation reconstruction + organic SEI	>3000 h @ 1 mA cm^{-2}/ 1 mAh cm^{-2}	V_2O_5: 89% after 500 and 80% after 800 cycles @ 0.5 A g^{-1}; cathode lading: 0.88 mg cm^{-2}; N/P ratio:157; electrolyte amount: 110 μL	[69]
O-Phosphorylethanolamine	P-rich organic-inorganic SEI + coordination	>3000 h @ 1 mA cm^{-2}	$NH_4V_4O_{10}$: 200 cycles@1 A g^{-1}; cathode lading: 1–2 mg cm^{-2}; electrolyte amount: 80 μL	[72]
$NH_4H_2PO_4$	Phosphate interphase + pH/desolvation regulation	CE-focused Zn plating test	31.2 mAh pouch: 400 cycles, 67.8% retention; areal capacity: 0.74 mAh cm^{-2}	[83]

3. Phosphate-Based Functional Interphases on Zn Metal

The solution chemistry discussed above can ultimately generate a phosphate-containing boundary at the Zn surface. Once formed, this interphase must satisfy two competing requirements. It should reduce direct contact between Zn and water, while remaining sufficiently permeable to Zn^{2+}. A highly blocking layer can suppress corrosion but increase interfacial resistance, whereas an overly permeable layer may provide little protection. Phosphate interphases are attractive because their thickness, structure, and surface chemistry can be tuned to balance these two requirements [87]. According to how they are generated, phosphate interphases can be broadly divided into preconstructed films and layers formed directly on Zn through interfacial reactions. Preconstructed films provide better control over the initial structure, whereas *in situ* formation allows the interface to develop in response to the local electrochemical environment. During repeated plating and stripping, both types may further evolve or reconstruct.

3.1. Preconstructed Phosphate Interphases

Preconstruction separates interphase fabrication from electrochemical operation, providing a direct way to control the initial thickness and structure of the protective layer. The central requirement is not simply to maximize passivation. The film must provide continuous coverage while maintaining a sufficiently short and accessible pathway for Zn^{2+} transfer. Li et al. demonstrated this principle using an amorphous zinc phosphate (AZP) nanofilm prepared at the air–water interface and subsequently transferred onto Zn [88]. A surfactant monolayer confined zinc-phosphate formation to the interface, producing a continuous ultrathin film rather than relying on direct reaction with metallic Zn. Structural characterization confirmed the formation of an amorphous phosphate phase, while the surfactant-derived outer surface exhibited reduced electrolyte wettability. Notably, the film exhibited an optimal thickness of approximately 24 nm, with thinner films providing insufficient coverage and thicker films increasing resistance to Zn^{2+} transfer [88]. This thickness dependence highlights the importance of balancing

interfacial protection with ionic accessibility. A similar thickness dependence has been observed for ultrathin zinc-phosphate coatings, further emphasizing that increasing the amount of phosphate does not necessarily improve Zn protection [89]. Other studies have introduced porosity, mixed-metal composition, or organic components to preserve ion accessibility while reducing direct exposure of Zn to the aqueous electrolyte [90–92]. These results collectively establish thickness and continuity as the first level of interphase design.

Beyond geometrical control, the chemical environment within the film can further regulate Zn deposition. Li et al. developed an amorphous Fe/Zn phosphate (FZP) nanofilm combining a hydrophobic outer surface with high surface charge [22]. The hydrophobic surface reduces direct electrolyte contact with reactive Zn sites, while the surface charge and phosphate composition further influence interfacial Zn deposition. Compared with bare Zn and single-metal phosphate interfaces, FZP/Zn maintained a more uniform deposited morphology under high-capacity plating conditions (Figure 2a,b). Calculations further revealed composition-dependent interactions between the phosphate layers and different Zn surfaces (Figure 2c,e,f), indicating that the interphase can influence Zn growth rather than acting only as a physical barrier. The advantage becomes more evident as the deposited capacity increases. At 20 mA cm^{-2}, the FZP-modified electrode sustained a deposition capacity of 64 mAh cm^{-2} before short circuit, compared with 22.7 mAh cm^{-2} for bare Zn (Figure 2d). The practical applicability of the FZP interphase was further demonstrated in Zn||I_2 full cells with high iodine loading and limited Zn inventory. With an iodine loading of 28 mg cm^{-2} and a 20-μm-thick Zn anode (N/P = 1.64), the full cell delivered an areal capacity of 6.37 mAh cm^{-2} and an electrode-based energy density of 176.5 Wh kg^{-1}, retaining 89.5% of its capacity after 250 cycles. Furthermore, pouch cells employing 50-μm-thick Zn anodes (N/P = 4.5) and the same iodine loading achieved an areal capacity of 5.12 mAh cm^{-2} and stable cycling over 200 cycles (Figure 2g). These results highlight the potential of phosphate interphases for high-loading Zn metal batteries.

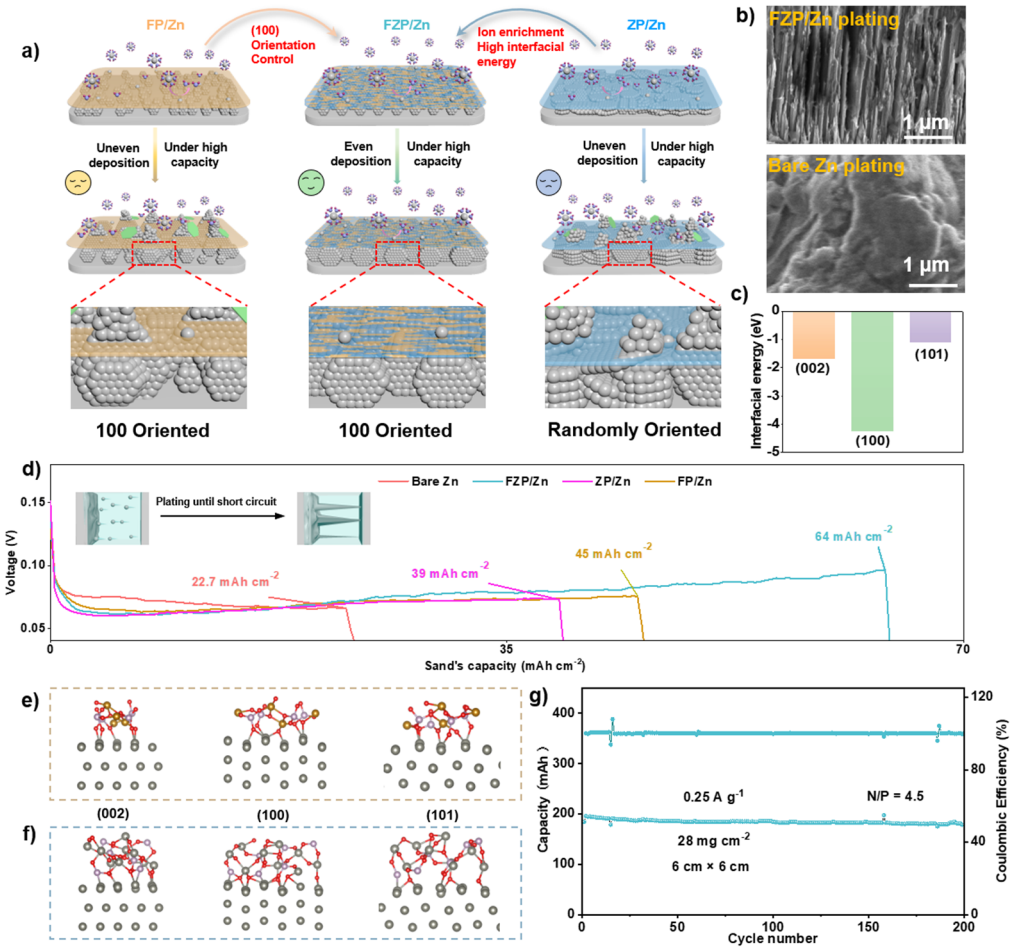

Figure 2. (**a**) Schematic of Zn electrodeposition behaviors on different electrodes; (**b**) SEM images of FZP/Zn and bare Zn electrodes after plating; (**c**) Calculated interfacial adsorption energies; (**d**) Voltage-areal capacity curves for symmetric cells with different electrodes at 20 mA cm^{-2}; Atomic structure of the interface between (**e**) FP and Zn, (**f**) ZP and Zn with different crystalline surfaces. (**g**) Cycling performance of pouch cells with high mass loading I_2 cathodes of 28 mg cm^{-2}. Reproduced with permission from Ref. [22]. Copyright 2025 Wiley-VCH GmbH.

Organic phosphate-derived interfaces offer another route to tune the boundary between Zn and the electrolyte. Phosphorylcholine-containing protective layers have been used to reduce parasitic reactions while maintaining Zn^{2+} transport [93]. Zinc-phytate-based interfaces introduce abundant phosphate-derived coordination sites and have been combined with porous or ion-selective components to regulate interfacial transport [94,95]. Phytic-acid conversion layers similarly form conformal phosphate-rich boundaries directly on Zn and improve plating/stripping stability without requiring a thick inorganic coating [96,97]. These studies reveal a common principle for preconstructed phosphate interphases. Effective protection requires a continuous but thin and ion-accessible boundary. Film thickness determines the transport distance, while composition and surface chemistry determine how water and Zn^{2+} interact with the interface. Increasing thickness, hydrophobicity, or binding strength alone is therefore insufficient. The most effective interphase is one that suppresses direct water-driven reactions while maintaining uniform Zn^{2+} transfer during repeated cycling.

3.2. In Situ Interphase Formation

In Situ formation provides a different route to phosphate protection because the interphase is generated directly on Zn rather than transferred as a preformed film. Its final structure therefore reflects the chemical environment under which it develops. Depending on the precursor and electrolyte, phosphate species can be converted near the electrode, precipitate after local supersaturation, or react with the native layer. Although these pathways may produce chemically similar phosphate-rich surfaces, their protective effects depend strongly on where and how the solid phase forms. Precursor conversion offers a relatively direct way to couple interphase formation with electrochemical operation. Molecular species can first accumulate near Zn and subsequently transform into less soluble phosphate-containing products as the interfacial environment changes [98−100]. For example, dimethyl methylphosphonate has been reported to form a monolithic interphase containing $Zn_3(PO_4)_2$ and ZnP_2O_6. The resulting Zn electrode sustained 4700 h of cycling and achieved a Zn/Cu Coulombic efficiency of 99.89% [101]. A second route is precipitation driven by the local environment during Zn deposition. Water reduction increases the interfacial pH, while changes in Zn^{2+} and phosphate activities can gradually bring the solution near the electrode to supersaturation [102–104]. Phosphate-rich nuclei can then form preferentially at the Zn surface and develop into a protective layer. The key requirement is spatial confinement. If the driving force is too weak, exposed Zn remains insufficiently protected; if it is too strong, precipitation extends into the bulk electrolyte or produces a thick layer that hinders Zn^{2+} transfer [105–107]. The useful regime therefore lies between these two limits, where interfacial precipitation is sufficient to cover reactive sites but stops before substantial transport resistance develops. The native Zn surface can also participate directly in interphase formation. Amorphous phosphate phases may form first and subsequently reorganize into more stable zinc-phosphate hydrates as hydration and local chemistry evolve [108]. Such conversion can preserve the spatial distribution of the native surface layer while replacing it with a more protective phosphate-containing boundary.

3.3. Dynamic Reconstruction of Phosphate Interphases

Phosphate interphases do not necessarily remain chemically unchanged during Zn plating and stripping. Changes in potential and local ion distribution can continuously alter the reactions occurring within the interphase and at the Zn surface [109]. Fu et al. demonstrated the dynamic reconstruction of a copper phosphate (CP) nanofilm on Zn [23]. XRD analysis confirmed the conversion of $Cu_3(PO_4)_2 \cdot 2H_2O$ into $Zn_3(PO_4)_2 \cdot 4H_2O$ after immersion in $ZnSO_4$ solution (Figure 3a–c). During Zn deposition, XPS measurements revealed an increased Zn^{2+} signal, a shift of Cu 2p features toward reduced Cu species, and the persistence of phosphate signals (Figure 3d–f), supporting the proposed Cu-to-Zn exchange and Cu reduction processes (Figure 3g). TEM/EDS characterization revealed the distribution of Cu and Zn, while additional SEM-EDS mapping showed preferential Cu enrichment at surface protrusions and grain boundaries (Figure 3h,i). These observations are consistent with localized Cu formation through galvanic replacement, although the preferential reaction kinetics at these sites were not directly measured. DFT calculations showed stronger Zn adsorption on amorphous copper phosphate than on bare Zn (−2.24 versus −0.55 eV), suggesting favorable Zn nucleation at the modified interface (Figure 3j). Furthermore, current-transient analysis indicated a transition from three-dimensional instantaneous nucleation on bare Zn to progressive nucleation on CP/Zn (Figure 3k,l). Together, these experimental observations and theoretical results support a proposed mechanism in which interphase reconstruction modifies the spatial distribution and nucleation behavior of Zn, thereby promoting more uniform deposition. The resulting electrode delivered an average Coulombic efficiency of 99.98% for more than 11,000 Zn||Cu cycles at 10 mA cm^{-2} and 1 mAh cm^{-2}. Its stability was further demonstrated in a 1.2 Ah Zn||I_2 pouch cell with an N/P ratio of 1.85 and an electrolyte usage of 20 μL mAh^{-1}.

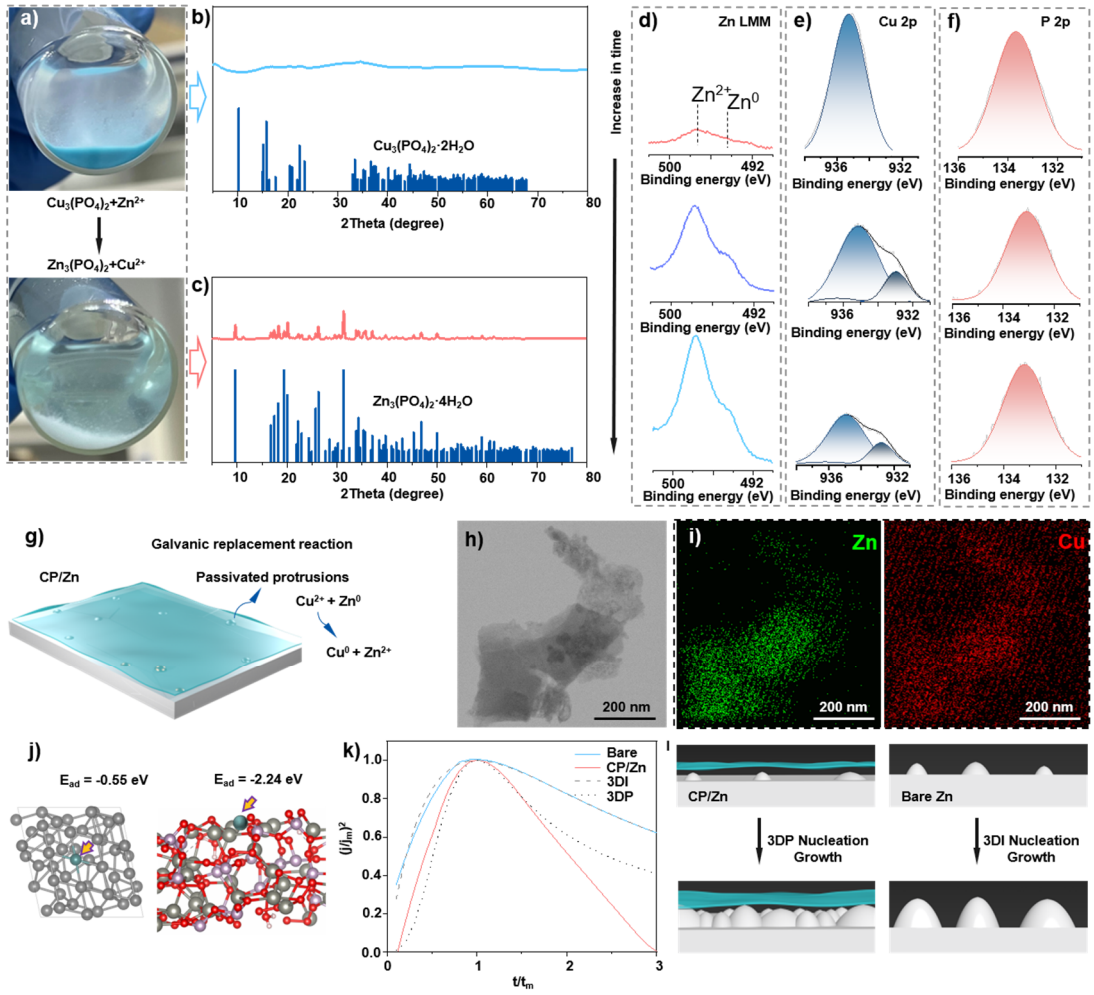

Figure 3. (**a**–**c**) Cu-to-Zn phosphate exchange after exposure of $Cu_3(PO_4)_2·2H_2O$ to $ZnSO_4$. (**d**–**f**) Evolution of the Zn LMM, Cu 2p, and P 2p spectra during Zn deposition, showing Zn incorporation and Cu^{2+} reduction while phosphate remains at the interface. (**g**) Schematic illustration of galvanic replacement and preferential Cu deposition at highly reactive Zn sites. (**h**,**i**) TEM image and elemental mapping after Zn deposition, showing the spatial distribution of Zn and Cu. (**j**) Calculated Zn adsorption configurations and adsorption energies on bare Zn and amorphous copper phosphate. (**k**,**l**) Current-transient curves and corresponding nucleation models, showing the transition from instantaneous to progressive Zn nucleation. Reproduced with permission from Ref. [23]. Copyright 2025 Wiley-VCH GmbH.

Electrolyte chemistry provides another route to control how an interphase develops during operation. Additives can simultaneously alter Zn^{2+} solvation and the species available for interphase formation, allowing the two processes to be regulated together [110]. The spatial distribution of these species can also be controlled. Electrolyte-mediated reactions have been used to generate composition gradients across Zn interphases [111], while deliberately imposed anion concentration gradients can direct where the interphase forms [112]. These studies illustrate a broader principle relevant to phosphate systems: interphase composition is determined not only by the final reaction product, but also by how reactive species are delivered to the Zn surface. For phosphate-containing systems, however, the detection of phosphorus after cycling alone is insufficient to establish a coupled electrolyte–interphase pathway. A convincing mechanism should connect the phosphate precursor in the electrolyte with the species formed at the surface and follow how this composition evolves during operation. The broader design target is therefore an adaptive but self-limiting interphase. A useful phosphate boundary should respond to newly exposed or highly reactive Zn sites without continuously thickening across the electrode. Once reconstruction becomes spatially uncontrolled, the same chemistry that initially protects Zn can consume electrolyte and increase Zn^{2+}-transfer resistance. Representative phosphate interphases and their electrochemical performance are summarized in Table 2.

Table 2. Electrochemical performance of representative phosphate-based Zn interphases.

System	Transport/Protection Evidence	Zn Test	Full-Cell/Practical Result	Ref.
FZP nanofilm	High surface charge compresses the EDL; hydrophobic outer face; Zn(100) orientation	Sand's capacity >64 mAh cm^{-2} at 20 mA cm^{-2}; >400 h at 2 mA cm^{-2} and 14 mAh cm^{-2} (60% DOD)	Zn‖I_2: N/P = 1.64, 176.5 Wh kg^{-1}; pouch cells up to 5.12 mAh cm^{-2}	[22]
CP/Zn	Galvanic replacement masks protrusions/grain boundaries; hydrophobic top layer limits water access	>11,000 Zn‖Cu cycles at 10 mA cm^{-2} and 1 mAh cm^{-2}, with an average CE of 99.98%	Zn‖I_2: N/P = 1.85, 187 Wh kg^{-1}; 1.2 Ah pouch cell	[23]
AZP nanofilm	Short isotropic paths; water shielding	3000 h @ 1 mA cm^{-2} and 500 h @ 50 mA cm^{-2}	MnO_2 full cell: 700 cycles under lean electrolyte/ limited Zn	[88]
PPA-Zn	Thickness-dependent ion conduction	6500 h @ 2 mA cm^{-2}; 6.5 Ah cm^{-2} cumulative	MnO_2: 78% after 500 cycles; V_2O_5 N/P = 4.26	[89]
CUPH-Zn	Zn affinity + hydrophobicity	700 h @ 0.8 mA cm^{-2}; 13.7% DOD	V_2O_5: >3500 cycles @ 2 A g^{-1}; N/P = 3.1	[90]
PZIL@Zn	Chelation + water exclusion	>1000 h @ 40 mA cm^{-2}; 74.3% DOD	Stable MnO_2 and activated-carbon devices at high rate	[93]
ZPHC@Zn	Desolvation + ion sieving	>3000 h at 1 mA cm^{-2} and 1 mAh cm^{-2}	V_2O_5: 75.1% after 1000 cycles @ 5 A g^{-1}	[94]
PA-Zn	Anticorrosion + lower desolvation barrier	>1400 h at 2 mA cm^{-2} and 1 mAh cm^{-2}	PANI@V_2O_5 full-cell validation	[97]
Monolithic SEI	Phosphate/boundary transport	4700 h	CE 99.89%; V_2O_5 82.2% after 4000 cycles @ 5 A g^{-1}	[101]
Fast-ion SEI	Intra-/intergranular transport; higher t_{Zn}	>4000 h @ 0.5 mA cm^{-2}; 2600 h @ 10 mA cm^{-2}; 13,000 cycles @ 40 mA cm^{-2}	Large-area pouch: 90.3% retention after 100 cycles	[107]

4. Phosphate-Containing Quasi-Solid Electrolytes

Phosphate chemistry can be extended from a nanometer-scale interphase into a continuous quasi-solid electrolyte. This change in length scale introduces a different design requirement. The material must not only regulate water near Zn, but also maintain continuous ion transport and intimate contact with a repeatedly plating and stripping metal surface. Most phosphate-containing quasi-solid electrolytes therefore rely on a hydrated polymer or hybrid network rather than a dry phosphate solid [113–116]. In these systems, phosphate groups mainly modify the state of the retained liquid and its interaction with Zn^{2+}, while the liquid fraction remains important for ion motion.

4.1. Network Formation and Water-State Regulation

In most phosphate-containing quasi-solid electrolytes, ion transport still occurs within a hydrated network. Phosphate groups alter this environment through interactions with water and Zn^{2+} rather than simply acting as independent conducting units. Their interaction with water can reorganize hydrogen bonding and change water retention, while their interaction with Zn^{2+} can modify the local coordination environment [117]. These effects become useful only within an intermediate regime. Weak interaction provides little control over the liquid phase, whereas excessive confinement can slow molecular exchange and increase polarization.

The PAM–PGO hydrogel reported by Abbasi et al. illustrates how phosphate functionalization can modify a hydrated network [118]. Phosphonated graphene oxide was incorporated into a polyacrylamide matrix, producing a lamellar composite structure with increased liquid retention. The ionic conductivity increased from 13.76 mS cm^{-1} for PAM to 20.81 mS cm^{-1} after addition of graphene oxide and further to 31.04 mS cm^{-1} after phosphonation. The PAM–PGO electrolyte also supported more stable Zn plating/stripping and improved full-cell cycling. These results show that phosphate functionalization can improve the transport environment of the retained liquid. A complementary strategy is to introduce a phosphate-containing molecule directly into the hydrated network. Shi et al. incorporated triethyl phosphate (TEP) into a polyacrylamide-based Zn electrolyte to regulate the hydrated network and Zn interfacial behavior [119]. FTIR analysis confirmed the formation of the polymer network and the incorporation of TEP (Figure 4a,b), while the crosslinked structure was proposed to regulate water through hydrogen-bonding interactions (Figure 4c). Electrochemical impedance measurements (Figure 4d) revealed ionic conductivities of 21.4 and 26.8 mS cm^{-1} for the TEP-containing sulfate and triflate hydrogels, respectively, compared with 7.12 mS cm^{-1} for the TEP-free sulfate hydrogel (Figure 4e). The TEP-containing electrolytes also exhibited broader apparent electrochemical stability windows (Figure 4f) and increased HER-related Tafel slopes (Figure 4g), suggesting suppressed water-driven side reactions. Furthermore, cyclic voltammetry revealed changes

in Zn nucleation behavior (Figure 4h), while polarization measurements indicated electrolyte-dependent corrosion behavior (Figure 4i). These results illustrate how phosphate-containing molecules can regulate the hydrated environment and interfacial electrochemistry within quasi-solid networks, although enhanced total ionic conductivity does not necessarily indicate faster Zn^{2+} transport.

These two examples highlight a common role of phosphate in quasi-solid electrolytes. Whether phosphate groups are anchored to a scaffold or introduced as molecular additives, their principal function is to reshape the hydrated phase through which ions move. Importantly, water regulation should not be equated with complete water exclusion. In hydrated networks, sufficient water mobility and electrolyte accessibility are required to support ion exchange, salt dissociation, and interfacial Zn^{2+} transfer, whereas excessive confinement may increase transport resistance and polarization. The objective is therefore to suppress water-driven parasitic reactions at the Zn surface while preserving continuous ionic pathways. Studies of water-shielding interfaces and interrupted hydrogen-bond networks further highlight the importance of regulating water availability rather than simply minimizing water content [120,121]. Because surface wettability alone cannot establish effective water shielding or efficient Zn^{2+} transport, this balance should be evaluated through interfacial impedance, polarization behavior, and Zn plating/stripping reversibility.

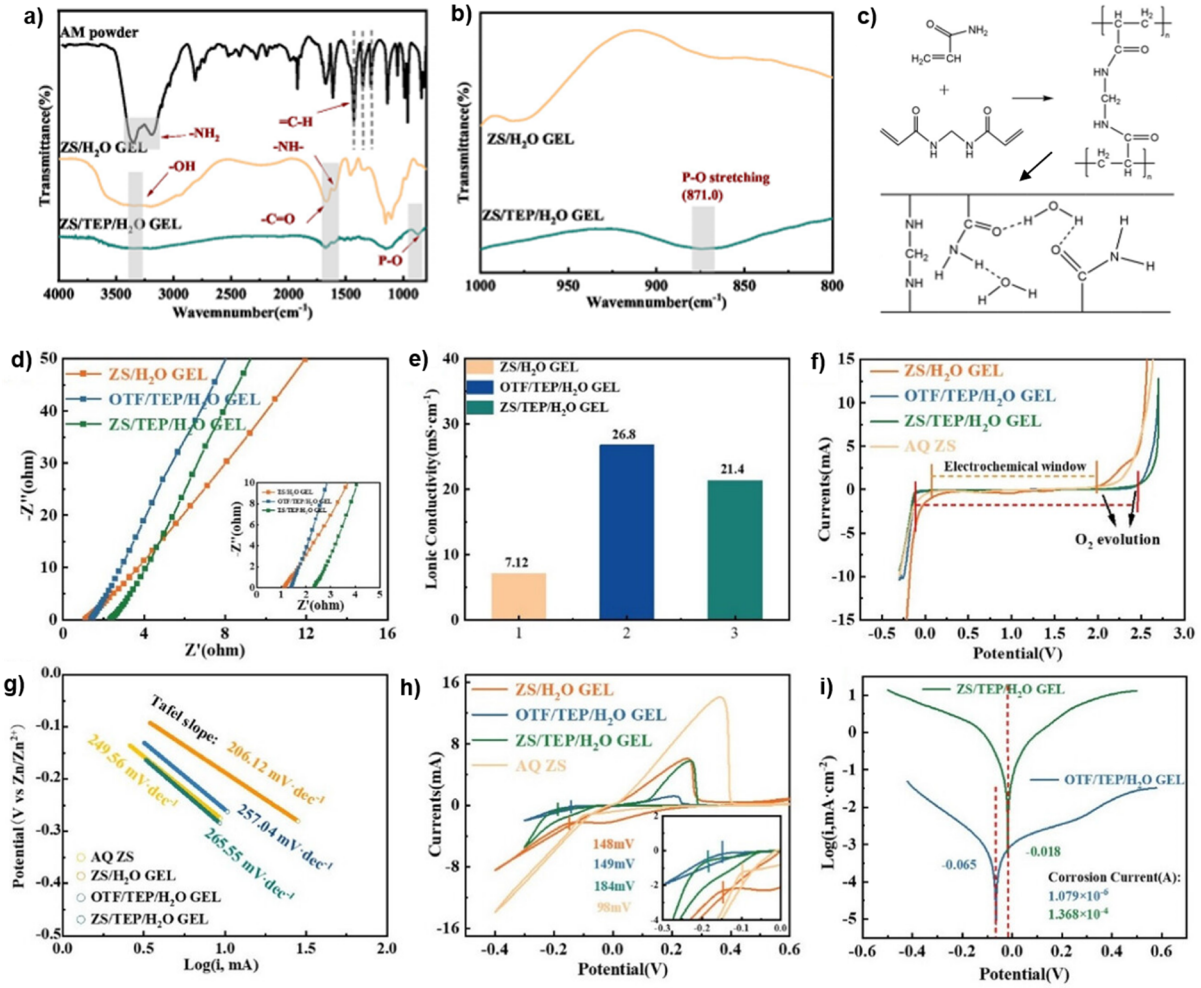

Figure 4. (**a**,**b**) FTIR profiles of the AM powder and electrolytes; (**c**) The polymerization mechanism diagram of the hydrogel electrolyte. (**d**) EIS spectrum of different hydrogel electrolytes; (**e**) ionic conductivity of the electrolytes; and (**f**) the LSV profiles and (**g**) corresponding Tafel plots of different electrolytes; (**h**) CV profiles of Zn//SS batteries with different electrolytes at a scan rate of 1 $mV \cdot s^{-1}$; (**i**) Tafel profiles of different hydrogel electrolytes. Reproduced with permission from Ref. [119]. Copyright 2025 Wiley-VCH GmbH.

4.2. Mechanical Continuity and Ion-Transport Pathways

Regulating the retained liquid is effective only when the quasi-solid network maintains structural continuity and intimate contact with Zn during repeated plating and stripping. Changes in electrode morphology require the network to accommodate interfacial deformation without disrupting ion-transport pathways. Although stronger

crosslinking can improve dimensional stability, excessive rigidity may compromise interfacial contact and restrict ionic mobility, whereas overly soft networks may undergo deformation and liquid redistribution. The key requirement is therefore to balance mechanical integrity, interfacial adaptability, and efficient ion transport. The porous metal–phosphonate–organic interfacial network reported by He et al. illustrates how phosphate-containing structures can limit water exposure while preserving accessible pathways for Zn^{2+} supply [122]. Although this structure is an interphase rather than a bulk quasi-solid electrolyte, it highlights the importance of maintaining both structural continuity and ionic accessibility.

Ion transport in phosphate-containing quasi-solid electrolytes depends strongly on the hydration environment and network structure. In water-rich hydrogels, Zn^{2+} migration is expected to occur primarily through connected liquid domains, while reduced liquid mobility may increase the influence of coordination interactions with nearby functional groups. In inorganic-rich phosphate phases, structural water, grain boundaries, and defects may also contribute to ionic transport. However, these pathways should not be automatically attributed to Zn^{2+} migration, as phosphate-based materials can also support proton conduction, particularly through hydrogen-bonded networks [123–133]. Even $Zn_3(PO_4)_2{\cdot}4H_2O$ has been reported to exhibit ionic conduction under hydrated conditions [134], although the measured conductivity alone does not establish the identity of the dominant charge carriers. Distinguishing Zn^{2+} transport from possible proton and anion contributions is therefore essential for understanding the conduction mechanisms of phosphate-containing networks.

Quantitative evaluation should combine total ionic conductivity with the Zn^{2+} transference number and independent assessment of proton transport. Temperature-dependent conductivity measurements can provide apparent activation energies, although these values alone cannot identify the mobile species. Mechanical properties, including storage and loss moduli, should be evaluated alongside water retention and water activity to assess network stability and ion accessibility. Furthermore, interfacial impedance measurements before and after cycling, together with polarization and Zn plating/stripping tests, can provide complementary information on interfacial contact and charge-transfer behavior. These parameters collectively establish a framework for evaluating how phosphate chemistry balances mechanical continuity, water regulation, and efficient Zn^{2+} transport in quasi-solid electrolytes.

5. Conclusions and Outlook

Phosphate chemistry offers a chemically continuous way to stabilize Zn metal across the electrolyte–electrode boundary. In solution, phosphate-containing species modify Zn^{2+} coordination, reorganize the local water environment and moderate interfacial pH changes. As the reaction proceeds toward the Zn surface, the same chemistry can drive adsorption, precipitation, conversion or reconstruction into protective phosphate-rich phases. In quasi-solid electrolytes, phosphate groups further regulate retained water and the pathways available for ion transport. The same principle holds across these regimes: phosphate interactions should be strong enough to suppress water-driven side reactions, yet dynamic enough to preserve rapid and uniform Zn^{2+} transfer. Phosphate chemistry is more than a collection of additives, coatings or functional groups; its distinctive value lies in evolving with the local electrochemical environment and thereby connecting solution regulation with interphase formation and ion transport.

On this basis, future work should focus on five interrelated priorities.

1. Phosphate can act as a soluble regulator, an interphase precursor or an undesirable precipitate depending on the local electrochemical environment. Studies should identify when these transitions occur during Zn plating and stripping, especially as local pH and Zn^{2+} activity evolve.
2. Phosphate interphases are better treated as dynamic structures than as static coatings. Tracking their evolution during cycling would show whether protection comes from persistent coverage, selective regulation of reactive sites or self-limiting reconstruction, and would help distinguish beneficial adaptation from uncontrolled thickening or precipitation.
3. High ionic conductivity alone does not prove Zn^{2+} conduction through a phosphate-containing network. Zn^{2+} transport needs to be separated from contributions of protons, anions and retained liquid, and ion motion should be connected directly to interfacial Zn plating and stripping.
4. Mechanisms established in Zn||Zn cells should be tested with limited Zn inventory, high cathode loading, lean electrolyte and eventually pouch-cell configurations. Only under these conditions can one judge whether phosphate-enabled protection remains effective as Zn and electrolyte resources become progressively limited.
5. The practical effectiveness of phosphate-enabled Zn protection should be further assessed using quantitative cell-level benchmarks rather than prolonged symmetric-cell cycling alone. Pouch-cell validation should also assess calendar stability over several months by monitoring recoverable capacity, self-discharge, corrosion, and gas evolution.

Author Contributions

X.L., Z.W. and T.G.: Writing—original draft preparation; Y.W. (Yingjin Wei) and Y.W. (Yizhan Wang): Supervision—reviewing and editing. All authors have read and agreed to the published version of the manuscript.

Funding

This work was supported by the Natural Science Foundation of Jilin Province (No. 20240101184JC), National Natural Science Foundation of China (No. 22279043), Fundamental Research Funds for the Central Universities, Jilin University.

Institutional Review Board Statement

Not applicable.

Informed Consent Statement

Not applicable.

Data Availability Statement

Date will be made available on request.

Conflicts of Interest

The authors declare no conflict of interest.

Use of AI and AI-Assisted Technologies

During the preparation of this work, the authors used DeepSeek to polish the language. After using this tool, the authors reviewed and edited the content as needed and takes full responsibility for the content of the published article.

References

1. Deng, Y.P.; Liang, R.; Jiang, G.; et al. The Current State of Aqueous Zn-Based Rechargeable Batteries. *ACS Energy Lett.* **2020**, *5*, 1665–1675. https://doi.org/10.1021/acsenergylett.0c00502.
2. Zhang, W.; He, G. Solid-Electrolyte Interphase Chemistries towards High-Performance Aqueous Zinc Metal Batteries. *Angew. Chem. Int. Ed.* **2023**, *62*, e202218466. https://doi.org/10.1002/anie.202218466.
3. Li, Y.; Yu, Z.; Huang, J.; et al. Constructing Solid Electrolyte Interphase for Aqueous Zinc Batteries. *Angew. Chem. Int. Ed.* **2023**, *62*, e202309957. https://doi.org/10.1002/anie.202309957.
4. Wang, L.; Liu, H.; Dou, S.X.; et al. Zinc Anode Stabilization in Aqueous Zinc-Ion Batteries: A Comprehensive Review of Challenges and Strategies. *Adv. Energy Mater.* **2026**, *16*, e70916. https://doi.org/10.1002/aenm.70916.
5. Anil Kumar, Y.; Mishra, V.; Ramachandran, T.; et al. Hybrid sodium-/zinc-ion battery systems: Emerging approaches for low-cost and safe energy storage. *Sustain. Energy Fuels* **2026**, *10*, 2383–2414. https://doi.org/10.1039/d6se00044d.
6. Prakash, T.; Govindan, R.; Leonardi, G.S.; et al. Design and construction of MoS_2@Carbon composite as a potential anode for sodium-ion batteries. *J. Sci. Adv. Mater. Devices* **2026**, *11*, 101178. https://doi.org/10.1016/j.jsamd.2026.101178.
7. Sanjana, S.; Siva, V.; Murugan, A.; et al. Hydrothermally Synthesized $Mn_2V_2O_7$ Nanopebble-Decorated ZIF-67: A Promising Cathode Material for Energy Storage Applications. *ACS Omega* **2026**, *11*, 18653–18663. https://doi.org/10.1021/acsomega.5c08239. Correction in *ACS Omega* **2026**, *11*, 26079. https://doi.org/10.1021/acsomega.6c03565.
8. Manikandan, R.; Raj, C.J.; Jung, H.; et al. Emerging intertwined nanofibers stabilized two-dimensional sodium vanadium pyrophosphate network for high-potential electrode in sodium-ion storage. *Chem. Eng. J.* **2025**, *525*, 170154. https://doi.org/10.1016/j.cej.2025.170154.
9. Chandra Mouli, K.V.V.; Reddy, N.P.; Ramachandran, T.; et al. Progress in anode engineering for rechargeable zinc-ion batteries: Strategies for dendrite suppression and host architectures. *Sustain. Energy Fuels* **2026**, *10*, 1579–1610. https://doi.org/10.1039/d6se00099a.
10. Duan, F.; Ba, J.; Wu, M.; et al. Near-Theoretical-Density Zinc Plating Enabled by an Ordered Janus Interphase for High-Energy Zinc Pouch Cells. *Nano Lett.* **2026**, *26*, 13517–13526. https://doi.org/10.1021/acs.nanolett.6c03595.
11. Xu, Z.; Li, J.; Fu, Y.; et al. Suppression of interfacial water layer with solid contact using an ultrathin, water-repellent, and Zn^{2+}-selective layer for Ah-level zinc metal batteries. *Energy Environ. Sci.* **2025**, *18*, 4251–4261. https://doi.org/10.1039/d4ee05905k.

12. Ba, J.; Li, X.; Li, J.; et al. Sustained Release of Underpotential Deposition Initiators for Ah-Level Zinc Metal Batteries. *Angew. Chem. Int. Ed.* **2025**, *64*, e202514181. https://doi.org/10.1002/anie.202514181.
13. Ba, J.; Li, X.; Li, J.; et al. An all-fluorinated interphase by Zn mediated reduction of organofluorine for a high energy Zinc metal pouch cell. *Energy Environ. Sci.* **2026**, *19*, 6164–6177. https://doi.org/10.1039/d6ee04249j.
14. Li, X.; Ba, J.; Li, J.; et al. Ultrahigh areal capacity aqueous zinc pouch cell enabled by proton scavengers. *Mater. Today* **2026**, *97*, 103372. https://doi.org/10.1016/j.mattod.2026.103372.
15. Zhao, Q.; Sun, Z.; Liu, H.; et al. A Systematic Understanding of Zinc Salts in Electrolyte Design for Aqueous Zinc-Ion Batteries. *ACS Nano* **2025**, *19*, 35237–35275. https://doi.org/10.1021/acsnano.5c10278.
16. Dong, D.; Zhao, C.X.; Zhang, X.; et al. Aqueous Electrolytes: From Salt in Water to Water in Salt and Beyond. *Adv. Mater.* **2025**, *37*, 2418700. https://doi.org/10.1002/adma.202418700.
17. Liu, J.; Peng, Z.; Liao, R.; et al. Electrolyte Additives for Enhanced Aqueous Zinc-Ion Battery Performance. *Batter. Supercaps* **2025**, *8*, e202500420. https://doi.org/10.1002/batt.202500420.
18. Wu, Z.; Huang, Z.; Zhang, R.; et al. Aqueous electrolyte additives for zinc-ion batteries. *Int. J. Extrem. Manuf.* **2024**, *6*, 062002. https://doi.org/10.1088/2631-7990/ad65ca.
19. Jayakumar, R.; Harrison, D.M.; Xu, J.; et al. Interphases in aqueous rechargeable zinc metal batteries. *J. Mater. Chem. A* **2023**, *11*, 8470–8496. https://doi.org/10.1039/d3ta00254c.
20. Lu, W.; Zhang, C.; Zhang, H.; et al. Anode for Zinc-Based Batteries: Challenges, Strategies, and Prospects. *ACS Energy Lett.* **2021**, *6*, 2765–2785. https://doi.org/10.1021/acsenergylett.1c00939.
21. Tu, H.; Li, X.; Zhou, Y.; et al. Enhancing Zn Anode Reversibility via Solvation Structure Reconstruction by a Trimethyl Phosphate Additive. *ACS Appl. Energy Mater.* **2024**, *7*, 4385–4393. https://doi.org/10.1021/acsaem.4c00244.
22. Li, J.; Ba, J.; Zhao, C.; et al. A Hydrophobic and High Surface Charge Phosphate Interphase for High Areal Capacity Zinc Metal Batteries. *Adv. Mater.* **2025**, *37*, 2501956. https://doi.org/10.1002/adma.202501956.
23. Fu, Y.; Li, J.; Wu, M.; et al. Selective Masking of Active Sites in Zinc Metal via Galvanic Replacement Reaction for Highly Reversible Ah-Level Zinc-I_2 Batteries. *Angew. Chem. Int. Ed.* **2025**, *64*, e202500731. https://doi.org/10.1002/anie.202500731.
24. Xu, X.; Xu, Y.; Zhang, J.; et al. Quasi-Solid Electrolyte Interphase Boosting Charge and Mass Transfer for Dendrite-Free Zinc Battery. *Nano-Micro Lett.* **2023**, *15*, 56. https://doi.org/10.1007/s40820-023-01031-7.
25. Yang, C.; Woottapanit, P.; Geng, S.; et al. A multifunctional quasi-solid-state polymer electrolyte with highly selective ion highways for practical zinc ion batteries. *Nat. Commun.* **2025**, *16*, 183. https://doi.org/10.1038/s41467-024-55656-2.
26. Guan, Y.; Hao, X.; Xu, R.; et al. Carbon Materials for Zinc-Iodine Battery Cathodes. *Prog. Chem.* **2025**, *37*, 775–787. https://doi.org/10.7536/pc240610.
27. Ye, M.; Guan, Y.; Xu, R.; et al. Aqueous potassium-ion battery cathodes: Current status and prospects. *J. Energy Chem.* **2025**, *106*, 650–670. https://doi.org/10.1016/j.jechem.2025.03.008.
28. Ran, Y.; Dong, F.; Sun, S.; et al. Aqueous Zinc-Based Batteries: Active Materials, Device Design, and Future Perspectives. *Adv. Energy Mater.* **2026**, *16*, 2406139. https://doi.org/10.1002/aenm.202406139.
29. Sun, Q.; Du, H.H.; Sun, T.J.; et al. Sorbitol-Electrolyte-Additive Based Reversible Zinc Electrochemistry. *J. Electrochem.* **2024**, *30*, 2314002. https://doi.org/10.61558/2993-074x.3447.
30. Yang, G.; Zhang, X.; Zhang, H.; et al. Hydrogen bond-anchored interfacial engineering for stable and high-performance aqueous zinc-ion batteries. *eScience Energy* **2026**, *2*, 100027. https://doi.org/10.1016/j.esen.2026.100027.
31. Zhang, M.; Hua, H.; Dai, P.; et al. Dynamically Interfacial pH-Buffering Effect Enabled by N-Methylimidazole Molecules as Spontaneous Proton Pumps toward Highly Reversible Zinc-Metal Anodes. *Adv. Mater.* **2023**, *35*, 2208630. https://doi.org/10.1002/adma.202208630.
32. Puyo-Fourtine, J.; Juillé, M.; Hénin, J.; et al. Consistent Picture of Phosphate–Divalent Cation Binding from Models with Implicit and Explicit Electronic Polarization. *J. Phys. Chem. B* **2022**, *126*, 4022–4034. https://doi.org/10.1021/acs.jpcb.2c01158.
33. Schauss, J.; Kundu, A.; Fingerhut, B.P.; et al. Contact Ion Pairs of Phosphate Groups in Water: Two-Dimensional Infrared Spectroscopy of Dimethyl Phosphate and ab Initio Simulations. *J. Phys. Chem. Lett.* **2019**, *10*, 6281–6286. https://doi.org/10.1021/acs.jpclett.9b02157.
34. Schauss, J.; Dahms, F.; Fingerhut, B.P.; et al. Phosphate–Magnesium Ion Interactions in Water Probed by Ultrafast Two-Dimensional Infrared Spectroscopy. *J. Phys. Chem. Lett.* **2019**, *10*, 238–243. https://doi.org/10.1021/acs.jpclett.8b03568.
35. Cong, J.; Wang, Y.; Lin, X.; et al. Kinetics Compensation Mechanism in Cosolvent Electrolyte Strategy for Aqueous Zinc Batteries. *J. Am. Chem. Soc.* **2025**, *147*, 8607–8617. https://doi.org/10.1021/jacs.4c16880.
36. Yu, X.; Chen, M.; Li, Z.; et al. Unlocking Dynamic Solvation Chemistry and Hydrogen Evolution Mechanism in Aqueous Zinc Batteries. *J. Am. Chem. Soc.* **2024**, *146*, 17103–17113. https://doi.org/10.1021/jacs.4c02558.
37. Zhang, Q.; Ma, Y.; Lü, Y.; et al. Designing Anion-Type Water-Free Zn^{2+} Solvation Structure for Robust Zn Metal Anode. *Angew. Chem. Int. Ed.* **2021**, *60*, 23357–23364. https://doi.org/10.1002/anie.202109682.

38. Cao, L.; Li, D.; Hu, E.; et al. Solvation Structure Design for Aqueous Zn Metal Batteries. *J. Am. Chem. Soc.* **2020**, *142*, 21404–21409. https://doi.org/10.1021/jacs.0c09794.
39. Wang, F.; Borodin, O.; Gao, T.; et al. Highly reversible zinc metal anode for aqueous batteries. *Nat. Mater.* **2018**, *17*, 543–549. https://doi.org/10.1038/s41563-018-0063-z.
40. Zhang, B.; Yao, J.; Wu, C.; et al. Electrolyte design for reversible zinc metal chemistry. *Nat. Commun.* **2025**, *16*, 71. https://doi.org/10.1038/s41467-024-55657-1.
41. Ming, F.; Zhu, Y.; Huang, G.; et al. Co-Solvent Electrolyte Engineering for Stable Anode-Free Zinc Metal Batteries. *J. Am. Chem. Soc.* **2022**, *144*, 7160–7170. https://doi.org/10.1021/jacs.1c12764.
42. Cigala, R.M.; Crea, F.; De Stefano, C.; et al. Quantitative study on the interaction of Sn^{2+} and Zn^{2+} with some phosphate ligands, in aqueous solution at different ionic strengths. *J. Mol. Liq.* **2012**, *165*, 143–153. https://doi.org/10.1016/j.molliq.2011.11.002.
43. Moe, O.A.; Wiest, S.A. Determination of stability constants for zinc-pyrophosphate complexes. *Anal. Biochem.* **1977**, *77*, 73–78. https://doi.org/10.1016/0003-2697(77)90291-3.
44. Kundu, A.; Fingerhut, B.P.; Elsaesser, T. Hydration structure and dynamics of phosphoric acid and its anions—Ultrafast 2D-IR spectroscopy and ab initio molecular dynamics simulations. *J. Chem. Phys.* **2024**, *161*, 084503. https://doi.org/10.1063/5.0216640.
45. Sharma, B.; Chandra, A. Ab Initio Molecular Dynamics Simulation of the Phosphate Ion in Water: Insights into Solvation Shell Structure, Dynamics, and Kosmotropic Activity. *J. Phys. Chem. B* **2017**, *121*, 10519–10529. https://doi.org/10.1021/acs.jpcb.7b06091.
46. Borah, S. Hydration Properties of $HnPO_{4n-3}$ (n = 0–3) from Ab Initio Molecular Dynamics Simulations. *J. Phys. Chem. B* **2020**, *124*, 5454–5464. https://doi.org/10.1021/acs.jpcb.0c01769.
47. Costard, R.; Tyborski, T.; Fingerhut, B.P.; et al. Ultrafast phosphate hydration dynamics in bulk H_2O. *J. Chem. Phys.* **2015**, *142*, 212406. https://doi.org/10.1063/1.4914152.
48. Śmiechowski, M.; Gojło, E.; Stangret, J. Systematic Study of Hydration Patterns of Phosphoric(V) Acid and Its Mono-, Di-, and Tripotassium Salts in Aqueous Solution. *J. Phys. Chem. B* **2009**, *113*, 7650–7661. https://doi.org/10.1021/jp810195h.
49. Pye, C.C.; Rudolph, W.W. An ab Initio, Infrared, and Raman Investigation of Phosphate Ion Hydration. *J. Phys. Chem. A* **2003**, *107*, 8746–8755. https://doi.org/10.1021/jp035594h.
50. Liu, R.; Li, X.; Peng, C.; et al. Long-Cycle Aqueous Zinc-Ion Batteries Enabled by Interfacial Engineering via Hydrogen-Bond Disruption and pH Stabilization. *ACS Appl. Mater. Interfaces* **2025**, *17*, 62228–62238. https://doi.org/10.1021/acsami.5c18678.
51. Zhang, W.; Dai, Y.; Chen, R.; et al. Highly Reversible Zinc Metal Anode in a Dilute Aqueous Electrolyte Enabled by a pH Buffer Additive. *Angew. Chem. Int. Ed.* **2023**, *62*, e202212695. https://doi.org/10.1002/anie.202212695.
52. Guo, Y.; Zhang, Y.; Bi, S.; et al. Achieving a stable zinc anode-electrolyte interface with multifunctional ammonium dihydrogen phosphate additive. *J. Power Sources* **2026**, *678*, 240117. https://doi.org/10.1016/j.jpowsour.2026.240117.
53. Bajda, T.; Rogowska, M.; Pawłowska, A. Synthesis and solubility of hopeite $Zn_3(PO_4)_2{\cdot}4H_2O$. *Mineralogia* **2023**, *54*, 78–81. https://doi.org/10.2478/mipo-2023-0008.
54. Nriagu, J.O. Solubility equilibrium constant of α-hopeite. *Geochim. Cosmochim. Acta* **1973**, *37*, 2357–2361. https://doi.org/10.1016/0016-7037(73)90284-6.
55. Bach, S.; Celinski, V.R.; Dietzsch, M.; et al. Thermally Highly Stable Amorphous Zinc Phosphate Intermediates during the Formation of Zinc Phosphate Hydrate. *J. Am. Chem. Soc.* **2015**, *137*, 2285–2294. https://doi.org/10.1021/ja5103663.
56. Maslyk, M.; Bach, S.; Li, W.; et al. Understanding the Stability and Recrystallization Behavior of Amorphous Zinc Phosphate. *J. Phys. Chem. C* **2021**, *125*, 2636–2647. https://doi.org/10.1021/acs.jpcc.0c09044.
57. Boonchom, B.; Baitahe, R.; Kongtaweelert, S.; et al. Kinetics and Thermodynamics of Zinc Phosphate Hydrate Synthesized by a Simple Route in Aqueous and Acetone Media. *Ind. Eng. Chem. Res.* **2010**, *49*, 3571–3576. https://doi.org/10.1021/ie901626z.
58. Andrunik, M.; Wołowiec, M.; Wojnarski, D.; et al. Transformation of Pb, Cd, and Zn Minerals Using Phosphates. *Minerals* **2020**, *10*, 342. https://doi.org/10.3390/min10040342.
59. Herrmann, R.; García-García, F.J.; Reller, A. Rapid degradation of zinc oxide nanoparticles by phosphate ions. *Beilstein J. Nanotechnol.* **2014**, *5*, 2007–2015. https://doi.org/10.3762/bjnano.5.209.
60. Clever, H.L.; Derrick, M.E.; Johnson, S.A. The Solubility of Some Sparingly Soluble Salts of Zinc and Cadmium in Water and in Aqueous Electrolyte Solutions. *J. Phys. Chem. Ref. Data* **1992**, *21*, 941–1004. https://doi.org/10.1063/1.555909.
61. Reichle, R.A.; McCurdy, K.G.; Hepler, L.G. Zinc Hydroxide: Solubility Product and Hydroxy-complex Stability Constants from 12.5–75 °C. *Can. J. Chem.* **1975**, *53*, 3841–3845. https://doi.org/10.1139/v75-556.
62. Wei, W.; Zhang, F.; Li, H.; et al. Modulating the solvation structure and electrode interface through phosphate additive for highly reversible zinc metal anode. *Chem. Eng. J.* **2024**, *485*, 149944. https://doi.org/10.1016/j.cej.2024.149944.
63. Qiu, B.; Xie, L.; Zhang, G.; et al. Toward reversible wide-temperature Zn storage by regulating the electrolyte solvation structure via trimethyl phosphate. *Chem. Eng. J.* **2022**, *449*, 137843. https://doi.org/10.1016/j.cej.2022.137843.

64. Naveed, A.; Yang, H.; Yang, J.; et al. Highly Reversible and Rechargeable Safe Zn Batteries Based on a Triethyl Phosphate Electrolyte. *Angew. Chem. Int. Ed.* **2019**, *58*, 2760–2764. https://doi.org/10.1002/anie.201813223.
65. Elsaesser, T.; Schauss, J.; Kundu, A.; et al. Phosphate Vibrations Probe Electric Fields in Hydrated Biomolecules: Spectroscopy, Dynamics, and Interactions. *J. Phys. Chem. B* **2021**, *125*, 3899–3908. https://doi.org/10.1021/acs.jpcb.1c01502.
66. Wang, S.; Wang, S.; Wei, Z.; et al. A parts-per-million scale electrolyte additive for durable aqueous zinc batteries. *Nat. Commun.* **2025**, *16*, 1800. https://doi.org/10.1038/s41467-025-56607-1.
67. Xiao, F.; Wang, X.; Sun, K.; et al. Zincophilic armor: Phytate ammonium as a multifunctional additive for enhanced performance in aqueous zinc-ion batteries. *Chem. Eng. J.* **2024**, *489*, 151111. https://doi.org/10.1016/j.cej.2024.151111.
68. Wang, P.; Zhou, H.; Zhong, Y.; et al. Dendrite-Free Zn Metal Anodes with Boosted Stability Achieved by Four-in-One Functional Additive in Aqueous Rechargeable Zinc Batteries. *Adv. Energy Mater.* **2024**, *14*, 2401540. https://doi.org/10.1002/aenm.202401540.
69. Zhu, J.; Shangguan, M.; Li, H.; et al. A non-flammable trimethyl phosphate-water hybrid electrolyte for highly reversible and long cycle life Zn-V_2O_5 batteries. *J. Energy Storage* **2025**, *139*, 118710. https://doi.org/10.1016/j.est.2025.118710.
70. Hu, J.; Li, C.; Li, T.; et al. Interfacial stabilization of zinc anodes via trimethyl phosphate-regulated Zn Li hybrid electrolytes. *Inorg. Chem. Commun.* **2025**, *181*, 115207. https://doi.org/10.1016/j.inoche.2025.115207.
71. Kim, M.; Lee, J.; Choi, J.W. Molecular Engineering of Hybrid Electrolytes for Aqueous Zinc Ion Batteries. *Adv. Energy Mater.* **2025**, *15*, e04692. https://doi.org/10.1002/aenm.202504692.
72. Yin, J.; Wu, Z.; Liu, H.; et al. Unveiling the potential of phosphate ester on electrolyte microstructure optimization and interface chemistry modulation for aqueous zinc ion batteries. *J. Energy Storage* **2025**, *140*, 119128. https://doi.org/10.1016/j.est.2025.119128.
73. Wei, C.; Zhou, Y.; Wang, X.; et al. An economic bifunctional electrolyte additive for highly reversible zinc anode. *Mater. Today Phys.* **2024**, *41*, 101356. https://doi.org/10.1016/j.mtphys.2024.101356.
74. Wu, M.; Su, W.; Wang, X.; et al. Long-Life Aqueous Zinc–Organic Batteries with a Trimethyl Phosphate Electrolyte and Organic Cathode. *ACS Sustain. Chem. Eng.* **2023**, *11*, 957–964. https://doi.org/10.1021/acssuschemeng.2c05410.
75. Yang, J.; Yang, W.; Xu, X.; et al. Simultaneously Regulating Solvation Structure and Interphase by Strong Donor Cosolvent for Stable Zn-Metal Batteries. *J. Phys. Chem. C* **2023**, *127*, 7078–7086. https://doi.org/10.1021/acs.jpcc.3c01386.
76. Gregory, K.P.; Elliott, G.R.; Robertson, H.; et al. Understanding specific ion effects and the Hofmeister series. *Phys. Chem. Chem. Phys.* **2022**, *24*, 12682–12718. https://doi.org/10.1039/d2cp00847e.
77. Marcus, Y. Effect of Ions on the Structure of Water: Structure Making and Breaking. *Chem. Rev.* **2009**, *109*, 1346–1370. https://doi.org/10.1021/cr8003828.
78. Yan, Y.; Jiao, Y.; Wu, P. Realizing High Performance Four-Electron Zinc-Iodine Batteries with Acidic Eutectic Electrolyte. *Angew. Chem. Int. Ed.* **2025**, *64*, e202515633. https://doi.org/10.1002/anie.202515633.
79. Li, M.; Wang, X.; Meng, J.; et al. Comprehensive Understandings of Hydrogen Bond Chemistry in Aqueous Batteries. *Adv. Mater.* **2024**, *36*, 2308628. https://doi.org/10.1002/adma.202308628.
80. Tian, Z.; Guo, W.; Shi, Z.; et al. The Role of Hydrogen Bonding in Aqueous Batteries: Correlating Molecular-Scale Interactions with Battery Performance. *ACS Energy Lett.* **2024**, *9*, 5179–5205. https://doi.org/10.1021/acsenergylett.4c02281.
81. Wang, Y.; Wang, Z.; Pang, W.K.; et al. Solvent control of water O−H bonds for highly reversible zinc ion batteries. *Nat. Commun.* **2023**, *14*, 2720. https://doi.org/10.1038/s41467-023-38384-x.
82. Miao, L.; Wang, R.; Di, S.; et al. Aqueous Electrolytes with Hydrophobic Organic Cosolvents for Stabilizing Zinc Metal Anodes. *ACS Nano* **2022**, *16*, 9667–9678. https://doi.org/10.1021/acsnano.2c02996.
83. Yang, W.; Zhu, R.; Wu, G.; et al. Enhanced kinetics and stability for aqueous Zn battery enabled by low-cost additive chemistry. *Energy Storage Mater.* **2024**, *65*, 103153. https://doi.org/10.1016/j.ensm.2023.103153.
84. Cong, G.; Yuanlong, E.; Li, S.; et al. "Zinc phosphate armor": Constructing a robust interphase with betaine phosphate additive for zinc metal anodes. *J. Energy Storage* **2026**, *153*, 120941. https://doi.org/10.1016/j.est.2026.120941.
85. Luo, B.; Jiang, B.; Chang, F.; et al. *In-Situ* detection of pH and dissolved oxygen in electrolyte of aqueous zinc-ion batteries. *Nat. Commun.* **2025**, *16*, 8462. https://doi.org/10.1038/s41467-025-63260-1.
86. Hao, M.; Zhou, J.; Deng, R.; et al. Orchestrating dual-interface stabilization via a threefold mechanistic synergy of aluminum dihydrogen phosphate for ultrastable aqueous zinc-ion batteries. *J. Mater. Chem. A* **2026**, *14*, 30620–30634. https://doi.org/10.1039/d6ta03126a.
87. Li, D.; Cao, L.; Deng, T.; et al. Design of a Solid Electrolyte Interphase for Aqueous Zn Batteries. *Angew. Chem. Int. Ed.* **2021**, *60*, 13035–13041. https://doi.org/10.1002/anie.202103390.
88. Li, J.; Yin, X.; Duan, F.; et al. Pure Amorphous and Ultrathin Phosphate Layer with Superior Ionic Conduction for Zinc Anode Protection. *ACS Nano* **2023**, *17*, 20062–20072. https://doi.org/10.1021/acsnano.3c05640.
89. Li, J.; Zheng, Z.; Yu, Z.; et al. Stable Zn electrodes enabled by an ultra-thin Zn phosphate protective layer. *J. Mater. Chem. A* **2023**, *11*, 3051–3059. https://doi.org/10.1039/d2ta09153d.

90. Bao, Q.; Gong, Z.; Wang, P.F.; et al. Alkaline Copper Phosphate Coating Exhibiting Zincophilic and Hydrophobic Characteristics Achieves High-Performance in Aqueous Zinc-Ion Batteries. *ACS Appl. Energy Mater.* **2025**, *8*, 6232–6243. https://doi.org/10.1021/acsaem.5c00836.
91. Song, X.; Bai, L.; Wang, C.; et al. Synergistic Cooperation of Zn(002) Texture and Amorphous Zinc Phosphate for Dendrite-Free Zn Anodes. *ACS Nano* **2023**, *17*, 15113–15124. https://doi.org/10.1021/acsnano.3c04343.
92. Yu, N.; Li, Y.; She, W.; et al. Binder-Free Sodium Zinc Phosphate Protection Layer Enabled Dendrite-Free Zn Metal Anode. *ACS Appl. Mater. Interfaces* **2022**, *14*, 50827–50835. https://doi.org/10.1021/acsami.2c13499.
93. Meng, Z.; Jiao, Y.; Wu, P. Alleviating Side Reactions on Zn Anodes for Aqueous Batteries by a Cell Membrane Derived Phosphorylcholine Zwitterionic Protective Layer. *Angew. Chem. Int. Ed.* **2023**, *62*, e202307271. https://doi.org/10.1002/anie.202307271.
94. Liu, K.; Sun, Y.; Zhang, Y.; et al. Constructing a Dual Interfacial Layer of Zinc Phytate and Halloysite Nanotubes with Enhanced Ion Sieving and Desolvation for an Ultrastable Zinc Metal Anode. *Energy Fuels* **2025**, *39*, 22680–22690. https://doi.org/10.1021/acs.energyfuels.5c04574.
95. Du, L.; Hou, X.; Yang, X.; et al. Dendrite-Free Zinc Deposition Induced by Zinc-Phytate Coating for Long-Life Aqueous Zinc Batteries. *Batter. Supercaps* **2022**, *5*, e202100376. https://doi.org/10.1002/batt.202100376.
96. Shi, W.; Song, Z.; Wang, J.; et al. Phytic acid conversion film interfacial engineering for stabilizing zinc metal anode. *Chem. Eng. J.* **2022**, *446*, 137295. https://doi.org/10.1016/j.cej.2022.137295.
97. Zhang, Y.; Peng, C.; Zeng, Z.; et al. Sustainable Phytic Acid–Zinc Anticorrosion Interface for Highly Reversible Zinc Metal Anodes. *ACS Appl. Mater. Interfaces* **2022**, *14*, 10419–10427. https://doi.org/10.1021/acsami.1c24288.
98. Ma, D.; Li, F.; Ouyang, K.; et al. An electrochemically driven hybrid interphase enabling stable versatile zinc metal electrodes for aqueous zinc batteries. *Nat. Commun.* **2025**, *16*, 4817. https://doi.org/10.1038/s41467-025-60190-w.
99. Li, A.; Hao, J.; Wu, K.; et al. Turning $Zn(PO_3)_2$-Enriched Inorganic/Organic Hybrid Interfacial Chemistry with Chelating Ligands toward Robust Aqueous Zn Anodes. *ACS Nano* **2025**, *19*, 13016–13028. https://doi.org/10.1021/acsnano.4c17583.
100. Liu, K.; Sun, Y.; Zhang, Y.; et al. *In Situ* constructing an organic-inorganic hybrid interphase of agarose/zinc phosphate for reversible and dendrite-suppressed zinc metal anodes. *J. Energy Storage* **2026**, *165*, 122437. https://doi.org/10.1016/j.est.2026.122437.
101. Liu, S.; Vongsvivut, J.P.; Wang, Y.; et al. Monolithic Phosphate Interphase for Highly Reversible and Stable Zn Metal Anode. *Angew. Chem. Int. Ed.* **2023**, *62*, e202215600. https://doi.org/10.1002/anie.202215600.
102. Zhang, S.; Ye, M.; Zhang, Y.; et al. Regulation of Ionic Distribution and Desolvation Activation Energy Enabled by In Situ Zinc Phosphate Protective Layer toward Highly Reversible Zinc Metal Anodes. *Adv. Funct. Mater.* **2023**, *33*, 2208230. https://doi.org/10.1002/adfm.202208230.
103. Xia, S.; Luo, Q.; Liu, J.; et al. *In Situ* Spontaneous Construction of Zinc Phosphate Coating Layer toward Highly Reversible Zinc Metal Anodes. *Small* **2024**, *20*, 2310497. https://doi.org/10.1002/smll.202310497.
104. Zeng, X.; Mao, J.; Hao, J.; et al. Electrolyte Design for *In Situ* Construction of Highly Zn^{2+}-Conductive Solid Electrolyte Interphase to Enable High-Performance Aqueous Zn-Ion Batteries under Practical Conditions. *Adv. Mater.* **2021**, *33*, 2007416. https://doi.org/10.1002/adma.202007416.
105. Wang, J.; Yan, K.; Qi, H.; et al. *In Situ* construction of multifunctional metaphosphate interphase enabling stable zinc anode with fast Zn^{2+} transport kinetics. *EES Batter.* **2026**, *2*, 210–219. https://doi.org/10.1039/d5eb00098j.
106. Li, X.; Li, X.; Teng, W.; et al. Synergistic Wood-Derived Carbon Host with *In Situ* Formed Zinc Phosphate Layer for Stable Aqueous Zinc-Ion Batteries. *Chem. A Eur. J.* **2026**, *32*, e03626. https://doi.org/10.1002/chem.202503626.
107. Ye, K.; Qiu, T.; Wan, J.; et al. Synergetic Effect of Multicomponent Phosphate and Rich Grain-Boundary in Solid/Electrolyte Interphase Boosts Rapid Ion Transport toward Fast Aqueous Zinc Metal Batteries. *Adv. Energy Mater.* **2025**, *15*, 2502125. https://doi.org/10.1002/aenm.202502125.
108. Xie, Z.L.; Zhu, Y.; Du, J.Y.; et al. *In Situ* converting the native passivation layer into a fast ion transport interphase to boost the stability of zinc anodes. *Green Energy Environ.* **2025**, *10*, 1559–1567. https://doi.org/10.1016/j.gee.2025.02.004.
109. Chen, C.; Long, Z.; Du, X.; et al. Interfacial ionic effects in aqueous zinc metal batteries. *Energy Storage Mater.* **2024**, *71*, 103571. https://doi.org/10.1016/j.ensm.2024.103571.
110. Tang, S.; Li, J.; Wang, T.; et al. Electrolyte additive screening for co-regulation of solvation and solid electrolyte interphase in aqueous zinc batteries. *Nat. Commun.* **2026**, *17*, 8463. https://doi.org/10.1038/s41467-026-73025-z.
111. Wang, W.; Chen, S.; Liao, X.; et al. Regulating interfacial reaction through electrolyte chemistry enables gradient interphase for low-temperature zinc metal batteries. *Nat. Commun.* **2023**, *14*, 5443. https://doi.org/10.1038/s41467-023-41276-9.
112. He, X.; Cui, Y.; Qian, Y.; et al. Anion Concentration Gradient-Assisted Construction of a Solid–Electrolyte Interphase for a Stable Zinc Metal Anode at High Rates. *J. Am. Chem. Soc.* **2022**, *144*, 11168–11177. https://doi.org/10.1021/jacs.2c01815.
113. Zhang, Z.; Mu, Y.; Xiao, L.; et al. Hydrogel Electrolytes for Zinc-Ion Batteries: Materials Design, Functional Strategies, and Future Perspectives. *Nano-Micro Lett.* **2026**, *18*, 139. https://doi.org/10.1007/s40820-025-01993-w.

114. Mao, L.; Li, G.; Zhang, B.; et al. Functional Hydrogels for Aqueous Zinc-Based Batteries: Progress and Perspectives. *Adv. Mater.* **2025**, *37*, 2416345. https://doi.org/10.1002/adma.202416345.
115. Zhu, Z.; Xiong, S.; Li, J.; et al. Hydrogel Polymer Electrolytes for Aqueous Zinc-Ion Batteries: Recent Progress and Remaining Challenges. *Batteries* **2025**, *11*, 380. https://doi.org/10.3390/batteries11100380. Correction in *Batteries* **2025**, *11*, 407. https://doi.org/10.3390/batteries11110407.
116. Wang, Z.; Li, H.; Tang, Z.; et al. Hydrogel Electrolytes for Flexible Aqueous Energy Storage Devices. *Adv. Funct. Mater.* **2018**, *28*, 1804560. https://doi.org/10.1002/adfm.201804560.
117. Herschke, L.; Enkelmann, V.; Lieberwirth, I.; et al. The Role of Hydrogen Bonding in the Crystal Structures of Zinc Phosphate Hydrates. *Chem. A Eur. J.* **2004**, *10*, 2795–2803. https://doi.org/10.1002/chem.200305693.
118. Abbasi, A.; Xu, Y.; Abouzari-Lotf, E.; et al. Phosphonated graphene oxide-modified polyacrylamide hydrogel electrolytes for solid-state zinc-ion batteries. *Electrochim. Acta* **2022**, *435*, 141365. https://doi.org/10.1016/j.electacta.2022.141365.
119. Shi, S.; Chen, M.; Huo, X.; et al. A Polyacrylamide-Based Zinc Sulfate Hydrogel Electrolyte Enhanced by Triethyl Phosphate toward Stable Zinc Ion Battery Anode. *ChemPhysChem* **2025**, *26*, e202500005. https://doi.org/10.1002/cphc.202500005.
120. Peng, Z.; Li, S.; Tang, L.; et al. Water-shielding electric double layer and stable interphase engineering for durable aqueous zinc-ion batteries. *Nat. Commun.* **2025**, *16*, 4490. https://doi.org/10.1038/s41467-025-59830-y.
121. Cao, L.; Li, D.; Soto, F.A.; et al. Highly Reversible Aqueous Zinc Batteries enabled by Zincophilic–Zincophobic Interfacial Layers and Interrupted Hydrogen-Bond Electrolytes. *Angew. Chem. Int. Ed.* **2021**, *60*, 18845–18851. https://doi.org/10.1002/anie.202107378.
122. He, X.; Qian, Y.; Wu, Y.; et al. Metal-Phosphonate-Organic Network as Ion Enrichment Layer for Sustainable Zinc Metal Electrode with High Rate Capability. *Angew. Chem. Int. Ed.* **2024**, *63*, e202411563. https://doi.org/10.1002/anie.202411563.
123. Fop, S.; Vivani, R.; Masci, S.; et al. Anhydrous Superprotonic Conductivity in the Zirconium Acid Triphosphate $ZrH_5(PO_4)_3$. *Angew. Chem. Int. Ed.* **2023**, *62*, e202218421. https://doi.org/10.1002/anie.202218421.
124. Ishiyama, T.; Yamaguchi, T.; Omata, T. Proton-conducting phosphate glass: Recent development as an electrolyte in intermediate temperature fuel cells. *J. Ceram. Soc. Jpn.* **2022**, *130*, 1–9. https://doi.org/10.2109/jcersj2.21110.
125. Yu, J.W.; Yu, H.J.; Ren, Q.; et al. Humidity-sensitive irreversible phase transformation of open-framework zinc phosphate and its water-assisted high proton conduction properties. *Dalton Trans.* **2021**, *50*, 8070–8075. https://doi.org/10.1039/d1dt00296a.
126. Matsuda, Y.; Nakajima, J.; Inoue, Y.; et al. Tunnel-Structured Phosphate Exhibiting High Proton Conductivity and Thermal Stability over a Wide Intermediate Temperature Range. *Inorg. Chem.* **2024**, *63*, 8018–8025. https://doi.org/10.1021/acs.inorgchem.3c04006.
127. Kawakami, Y.; Miyayama, M. Proton Conducting Properties of Layered Metal Phosphate Hydrates. *Key Eng. Mater.* **2006**, *320*, 267–270. https://doi.org/10.4028/www.scientific.net/kem.320.267.
128. Ren, W.B.; Sun, S.; Gao, Z.; et al. Synthesis of Phosphovanadate-Based Porous Inorganic Frameworks with High Proton Conductivity. *Inorg. Chem.* **2023**, *62*, 20506–20512. https://doi.org/10.1021/acs.inorgchem.3c03703.
129. Zhang, K.M.; Ji, M.F.; Zhou, X.Y.; et al. The proton conduction behavior of two 1D open-framework metal phosphates with similar crystal structures and different hydrogen bond networks. *RSC Adv.* **2023**, *13*, 12703–12711. https://doi.org/10.1039/d3ra01130e.
130. Karafiludis, S.; Bhattacharya, B.; Buzanich, A.G.; et al. Thermally processed Ni-and Co-struvites as functional materials for proton conductivity. *Dalton Trans.* **2023**, *52*, 8262–8274. https://doi.org/10.1039/d3dt00839h.
131. Wang, S.; Xie, F.; Zhang, S.; et al. Water-assisted proton conduction regulated by hydrophilic groups in metallo-hydrogen-bonded organic frameworks: "like-attracts-like" between hydrophilic groups and water molecules. *CrystEngComm* **2023**, *25*, 4701–4715. https://doi.org/10.1039/d3ce00438d.
132. Mileo, P.G.M.; Kundu, T.; Semino, R.; et al. Highly Efficient Proton Conduction in a Three-Dimensional Titanium Hydrogen Phosphate. *Chem. Mater.* **2017**, *29*, 7263–7271. https://doi.org/10.1021/acs.chemmater.7b01850.
133. Colodrero, R.M.P.; Olivera-Pastor, P.; Cabeza, A.; et al. Properties and Applications of Metal Phosphates and Pyrophosphates as Proton Conductors. *Materials* **2022**, *15*, 1292. https://doi.org/10.3390/ma15041292.
134. Shin, W.; Lee, J.; Kim, Y.; et al. Ionic Conduction in $Zn_3(PO_4)_2 \cdot 4H_2O$ Enables Efficient Discharge of the Zinc Anode in Serum. *J. Am. Chem. Soc.* **2005**, *127*, 14590–14591. https://doi.org/10.1021/ja0556068.